International Journal of Computational Fluid Dynamics, April 2004 VOL. 18 (3), pp. 277–287

Taylor & Francis
Taylor & Francis Group

Space–Time Method for Detonation Problems with Finite-rate Chemical Kinetics

YUHUI WU, FUHUA MA and VIGOR YANG*

The Pennsylvania State University, 104 Research Building East, University Park, PA 16802, USA

(Received 10 November 2002; Revised 9 July 2003; In final form 9 July 2003)

The space–time conservation element and solution element (CE/SE) method originally developed for non-reacting flows is extended to accommodate finite-rate chemical kinetics for multi-component systems. The model directly treats the complete conservation equations of mass, momentum, energy, and species concentrations. A subtime-step integration technique is established to handle the stiff chemical source terms in the formulation. In addition, a local grid refinement algorithm within the framework of the CE/SE method is incorporated to enhance the flow resolution in areas of interest. The capability and accuracy of the resultant scheme are validated against several detonation problems, including shock-induced detonation with detailed chemical kinetics and multi-dimensional detonation initiation and propagation.

Keywords: Space–time method; Chemically reacting flows; Sub-time step integration algorithm; Detonation initiation and propagation

NOMENCLATURE

C	species mass concentration
C_p	constant-pressure specific heat
e	specific internal energy
e_t	specific total internal energy
E	convective flux vector in x-direction
Ea	activation energy in ZND model
F	convective flux vector in y-direction
H	source term vector
H_a	axisymmetric source term vector
H_c	chemical source term vector
k_b	chemical reaction rate
k_c	equilibrium constant for concentration
k_f	forward reaction rate
K	pre-exponential factor in ZND model
MW_j	molecular weight of species j
n_j	molar concentration of species j
p	pressure
q	heat release per unit mass of reactant
Q	dependent variable vector
t	time
T	temperature
u	axial velocity component
v	vertical or radial velocity component
x	axial coordinate
y	vertical or radial coordinate
Y	species mass fraction
Z	reactant mass fraction in ZND model

Subscripts

i	species index
n	time-step index

Greek Symbols

γ	specific heat ratio

---

*Corresponding author. Tel.: +1-814-863-1502. Fax: +1-814-865-3389. E-mail: vigor@psu.edu

ISSN 1061-8562 print/ISSN 1029-0257 online
DOI: 10.1080/10618560310001623340

ρ	density of gas mixture
ν'_{ij}	stoichiometric coefficient for species j appearing as reactant in ith forward reaction
ν''_{ij}	stoichiometric coefficient for species j appearing as reactant in ith backward reaction
$\dot{\omega}$	mass production rate

INTRODUCTION

Numerical simulations of chemically reacting flows often encounter severe difficulties due to the stiffness of source terms. The disparity of system eigenvalues and the involvement of a wide range of length and time scales pose another serious challenge (Hsieh and Yang, 1997). Existing methods for reacting-flow simulations can be divided into two categories. The first is the splitting method, in which the original governing equations are divided into two sets. One represents pure hydrodynamics without chemical source terms, and the other treats motionless chemical reactions (Boris and Oran, 2001). Numerical schemes developed for non-reacting flows, such as total variation diminishing (TVD) schemes (Harten, 1984) and flux-corrected transport (FCT) algorithms (Boris and Book, 1973), can be directly employed to solve the hydrodynamic set without modifications. The effects of chemical reactions are then taken into account by incorporating an ordinary differential equation (ODE) solver into the code. Since many well-developed stiff ODE solvers are available, the splitting method has been extensively used for problems involving strong chemical reactions. In particular, it is commonly used with the TVD and FCT schemes to solve detonation problems (Li *et al.*, 2000). The alternate solution procedure, however, may cause difficulties in enforcing conservation laws and consequently give rise to non-physical oscillations, as discussed by LeVeque and Yee (1990).

The second category of reacting-flow simulation is the direct method, which attempts to solve the entire system of governing equations in a coupled manner. Numerical schemes of this type have evolved from their non-reacting counterparts with the inclusion of chemical source terms. For example, Shuen *et al.* (1990) extended several inviscid flux-splitting algorithms for real gases with non-equilibrium chemistry. An upwind method was later developed by Shuen (1992) to solve chemical non-equilibrium Navier–Stokes equations. In an effort to handle flows over a wide range of Mach number, a series of preconditioning methods based on flux-differencing upwind TVD schemes was developed for the conservation laws with finite-rate chemical kinetics (Shuen *et al.*, 1993; Hsieh and Yang, 1997).

Both the splitting and direct methods based on upwind schemes require very complicated solution procedures. Basically, three common steps are involved: (i) the reconstruction step, in which the flow property distribution is approximated by polynomial curve fitting within each spatial conservation cell; (ii) an upwind step, in which an approximate Riemann solver is employed to calculate fluxes at cell interfaces; and (iii) the temporal evolution step, in which flow properties at the next time step are determined by means of either finite-difference methods or space–time flux conservation. For second- and higher-order upwind schemes, *ad-hoc* methods, such as flux and slope limiters, must be employed to suppress numerical oscillations. This inevitably complicates numerical coding and increases the computational burden due to the large number of logic operations (e.g., the [minmod] operation). Moreover, strict upwind biasing is not applicable to multi-dimensional problems in which directional splitting must be adopted. For flows containing discontinuities, some underlying assumptions, such as the monotonicity property of TVD schemes, may not be valid due to the presence of source terms.

In view of the deficiencies of existing schemes, the present work attempts to develop an efficient algorithm for chemically reacting flows involving shock and contact discontinuities based on the space–time conservation-element (CE) and solution element (SE) method (abbreviated as the space–time method) (Chang, 1995; Chang *et al.*, 1998; 1999), which was originally developed for non-reacting flows. Compared with conventional numerical algorithms, the space–time method has several unique features. First, the integral form of conservation laws are enforced in the space–time domain, such that flow quantities remain strictly conservative both locally and globally. Second, no Riemann solvers are employed in calculating fluxes. Instead, a zigzag marching strategy is proposed in the space–time domain, and the fluxes are naturally balanced with careful selection of spatial locations of conservation cells. This strategy is applicable to multi-dimensional flows, not just to one-dimensional cases. Consequently, the space–time method is a genuine multi-dimensional paradigm for solving conservation laws. Third, the space–time method is designed in such a manner that the inner structure of the flow solution in any given conservation cell is not constructed through curve-fitting over its neighbors. Instead, the gradients of flow variables are treated as independent unknowns, which evolve in time along with flow variables. In other words, the solution structure is not influenced by its neighboring values at the same time level. The resultant method is compact and is in full compliance with the flow physics for initial-value problems. Even though nominally it is only of second order of accuracy in both space and time, the space–time method generally exhibits an accuracy comparable to 4–6th-order compact difference schemes when nonlinear Euler problems are modeled (Loh *et al.*, 1996; Chang *et al.*, 1997). This is mainly due to the strict flux conservation property of the space–time method. In addition, the space–time method has very small dispersion errors in non-linear calculations, which also enhances its accuracy.

In an effort to extend the space–time method to treat flows involving strong source terms, Yu and Chang (1997) solved a one-dimensional Zeldovich, von Neumann, and Döring (ZND) detonation problem in which the chemical kinetics was approximated with a one-step global reaction. The chemical source term was treated implicitly, and a local Newton-Raphson iteration was adopted to determine the reactant mass concentration at each new time step. The method may, however, encounter convergence difficulty when applied to multi-component systems with second- or higher-order chemical reactions. To circumvent this problem, a subtime-step technique for multi-component chemically reacting systems was developed by Wu *et al.* (1999). The scheme accommodates property variations and detailed reaction mechanisms. The same idea was later adopted by Yu *et al.* (1999) and Guo *et al.* (2000). The former conducted subtime-step integration by using the trapezoidal rule along with a linearization procedure. The latter integrated source terms using an adaptive multi-step procedure, but very limited test cases were reported. The present work attempts to optimize the sub-time step integration technique developed by Wu *et al.* (1999) for treating chemical source terms within the context of the space–time method. To enhance computational efficiency, a local mesh refinement (Chang *et al.*, 2001) is incorporated to resolve steep gradients of flow properties associated with chemical reactions and shock discontinuities. The scheme is validated against several hydrogen/oxygen detonation problems with detailed chemical kinetics.

THEORETICAL FORMULATION

Governing Equations

The formulation is based on the conservation equations of mass, momentum, energy, and species concentrations for a chemically reacting system of N_s species. Full account is taken of finite-rate chemical kinetics and variable properties. If diffusive transport is ignored for detonation problems, the vector form of the inviscid part of the conservation laws can be rewritten as follows.

$$\frac{\partial y^{\delta}Q}{\partial t}+\frac{\partial y^{\delta}E}{\partial x}+\frac{\partial y^{\delta}F}{\partial y}=H \tag{1}$$

where $\delta = 0$ for planar two-dimensional and $\delta = 1$ for axisymmeric coordinates, respectively. The dependent variable vector, Q, and convective flux vectors in the x- and y-directions, E and F, are defined as follows.

$$Q=\begin{bmatrix}\rho\\ \rho u\\ \rho v\\ \rho e_t\\ C_1\\ C_2\\ \vdots\\ C_{N_s-1}\end{bmatrix},\quad E=\begin{bmatrix}\rho u\\ \rho u^2+p\\ \rho uv\\ \rho u(e_t+p/\rho)\\ uC_1\\ uC_2\\ \vdots\\ uC_{N_s-1}\end{bmatrix},$$

$$F=\begin{bmatrix}\rho v\\ \rho uv\\ \rho v^2+p\\ \rho v(e_t+p/\rho)\\ vC_1\\ vC_2\\ \vdots\\ vC_{N_s-1}\end{bmatrix}. \tag{2}$$

The source term vector, H, contains contributions from chemical reactions, H_c, and axisymmetric geometry, H_a.

$$H = H_c + H_a \tag{3}$$

where

$$H_c \equiv y^{\delta}\left[0,0,0,0,\dot{\omega}_1,\dot{\omega}_2,\cdots,\dot{\omega}_{N_s-1}\right]^T \quad \text{and}$$

$$H_a \equiv \delta\left[0,0,p,0,0,0,\cdots,0\right]^T.$$

The superscript T denotes a matrix transpose operation. In the above equations, ρ, u, v, C_i ($i = 1$, $N_s - 1$), p, and $\dot{\omega}_i$ are the density, velocity components in the x- and y-directions, mass concentration of species i, pressure, and mass production rate of species i per unit volume, respectively. The specific total energy, e_t, is defined as

$$e_t = e + \frac{1}{2}(u^2 + v^2). \tag{4}$$

The specific internal energy of the mixture, e, is defined as

$$\rho e = \sum_{i=1}^{N_s} C_i \left(\int_{T_{\text{ref}}}^{T} C_{p_i}\, dt + h_{f,i}^0 \right) - p \tag{5}$$

where C_{p_i} and $h_{f,i}^0$ are the constant-pressure specific heat and the heat of formation of species i, respectively.

Chemical Kinetics Model

For a set of N_R elementary reactions involving N_s species, the reaction equations can be written in the following general form.

$$\sum_{j=1}^{N_s} \nu'_{ij} M_j \Leftrightarrow \sum_{j=1}^{N_s} \nu''_{ij} M_j, \quad i = 1, \cdots, N_R \tag{6}$$

where ν'_{ij} and ν''_{ij} are the stoichiometric coefficients for species j appearing as a reactant in the ith forward and backward reactions, respectively. M_j is the chemical symbol for species j. The mass production rate of species j can be calculated from the following equation,

$$\dot{\omega}_j = \dot{n}_j \,\mathrm{MW}_j \tag{7}$$

where the rate of change of molar concentration of species j, $\dot{n}_j$, takes the form

$$\dot{n}_j = \sum_{i=1}^{N_R} \left(\nu''_{ij} - \nu'_{ij} \right) \left(k_{fi} \prod_{l=1}^{N_s} n_l^{\nu''_{ij}} - k_{bi} \prod_{l=1}^{N_s} n_l^{\nu'_{ij}} \right), \tag{8}$$

$$j = 1, \cdots, N_s.$$

The forward reaction rate constant of reaction i, k_{fi}, is obtained empirically using the Arrhenius expression

$$k_{fi} = A_{f,i} T^{m_{f,i}} \exp(-E_{f,i}/R_u T) \tag{9}$$

where $E_{f,i}$ is the activation energy, $A_{f,i}$ the pre-exponential factor, and $m_{f,i}$ the temperature constant. The backward reaction constant of reaction i, k_{bi}, can be calculated using the corresponding forward reaction rate and the equilibrium constant for species concentration, k_{ci},

$$k_{bi} = \frac{k_{f,i}}{k_{ci}}. \tag{10}$$

It should be noted that Eq. (8) is valid strictly for elemental reactions. If a global kinetics scheme is used, the exponents for molar concentrations may be varied from their stoichiometric coefficients in order to match experimental data.

NUMERICAL SCHEME

Space–Time Integration in One Spatial Coordinate

We start with one-dimensional problems to illustrate the main features of the space–time integration technique. The governing equation, Eq. (1), reduces to

$$\frac{\partial Q}{\partial t} + \frac{\partial E}{\partial x} = H. \tag{11}$$

Following the approach developed by Chang (1995), we define $\vec{h} = (E, Q)$ as the current density vector in a two-dimensional Euclidean sub-space $E_2 = (x, t)$. By applying Gauss' divergence theorem in the E_2-space, Eq. (11) is shown to be the differential form of the integral conservation law

$$\oint_{S(V)} \vec{h} \cdot d\vec{s} = \int_V H\, dV \tag{12}$$

where $S(V)$ is the boundary of an arbitrary space–time domain V in the E_2-space, and $d\vec{s} = d\sigma\vec{n}$, with $\vec{n}$ being the outward normal vector.

To proceed, we define the area $ABCDEFG$ in Fig. 1 as the conservation element CE(j,n) (Yu and Chang, 1997). The corresponding solution element, SE(j, n), is chosen to be coincident with CE(j,n). The distributions of $Q(x,t)$ and $E(x,t)$ within SE(j,n) are assumed to be continuous and approximated by first-order Taylor expansions about point A, whose grid index is (j, n). $Q(x, t)$ and $E(x, t)$ are further required to satisfy the differential form of the governing equations. Let s_j be the length of line segment $\overline{BF}$. The indices of grid points C and E are denoted as $(j_1, n-1)$ and $(j_2, n-1)$, respectively. Let $s_j^{(r)}$ $(r = 1, 2)$ be the lengths of line segments $\overline{CD}$ and $\overline{DE}$, respectively. Obviously, $s_j = \sum_{r=1}^{2} s_j^{(r)}$. We further define $\Delta\vec{s}_j^{(r)} = (\mp\Delta t, 0)$ $(r = 1, 2)$ as the outward vectors of the side faces $\overline{CB}$ and $\overline{EF}$ of conservation element CE(j,n), respectively.

Let $\vec{h}_j^{(r)} = (E_j^{(r)}, Q_j^{(r)})$ be the current-density vector $\vec{h}$ defined on the geometrical center of side face r

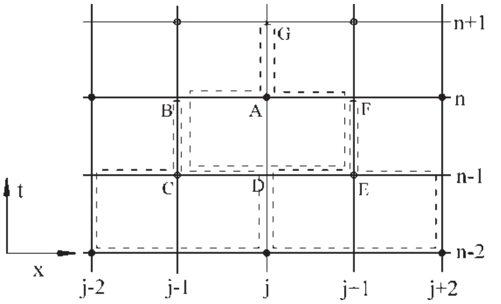

FIGURE 1 Conservation element and solution element in CE/SE method.

($r = 1, 2$). Since $\overline{CB}$ and $\overline{EF}$ belong to SE($j-1$, $n-1$) and SE($j+1$, $n-1$), respectively, $\vec{h}_j^{(r)}$ can be readily expressed as functions of quantities at points C and E, respectively, whose values are at ($n-1$)th time step. Therefore, $\vec{h}_j^{(r)}$ ($r = 1, 2$) are known. Enforcement of the conservation law, Eq. (12), on CE(j,n) then leads to the following result

$$(Q)_j^n - \frac{1}{s_j} \int_{CE(j,n)} H \, \mathrm{d}V = \mathrm{RHS} \tag{13}$$

where

$$\mathrm{RHS} \equiv \frac{1}{s_j} \left[\sum_{r=1}^{2} Q_{j_r}^{n-1} s_j^{(r)} - \sum_{r=1}^{2} \vec{h}_j^{(r)} \cdot \Delta\vec{s}_j^{(r)} \right] \tag{14}$$

and

$$\vec{h}_j^{(r)} \cdot \Delta\vec{s}_j^{(r)} = \mp \Delta t E_j^{(r)} \quad (r = 1, 2). \tag{15}$$

The term $E_j^{(r)}$ in Eq. (15) is approximated using the first-order Taylor expansion about point (x_{j_r}, t^n):

$$E_j^{(r)} = E_{j_r}^{n-1} + (e_\mathrm{t})_{j_r}^{n-1} \cdot \Delta t/2. \tag{16}$$

Those terms on the right-hand side of Eq. (13) take values at the last time step and thus are known quantities. Since the source-term vector H is a function of Q, Eq. (13) can be solved to obtain $(Q)_j^n$. The spatial derivative, $(Q_x)_j^n$, can then be evaluated using an oscillation-suppressing procedure developed by Chang (1995).

Space–Time Integration in Axisymmetric Coordinates

The space–time integration of the Euler equations in axisymmetric coordinates was developed by Wang and Chang (1999). The integration procedure is basically identical to that for spatially one-dimensional problems. Therefore, only a brief description is given here. More detailed information about the solution technique can be found in Wang and Chang (1999).

Let $x_1 = x$, $x_2 = y$, and $x_3 = t$ be the coordinates of a three-dimensional Euclidean space E_3. The integral form of Eq. (1) in the E_3-space becomes

$$\oint_{s(V)} \vec{h} \cdot \mathrm{d}\vec{s} = \int_V H \, \mathrm{d}V \tag{17}$$

where $s(V)$ is the boundary of an arbitrary space–time domain V in the E_3-space. The space–time current density vector $\vec{h}$ is defined as $\vec{h} = (E, F, Q)$.

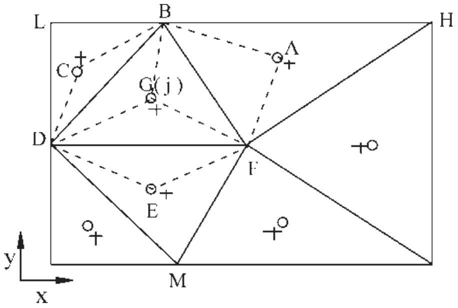

FIGURE 2 An arbitrary 2-D spatial domain formed by unstructured triangles.

Figure 2 shows an unstructured triangular mesh for a fluid flow problem with an arbitrary physical domain. The points marked by circles denote the centroids of the triangles in which they reside, while the points marked by crosses are defined as the solution points of the corresponding triangles and are located at the centroids of hexagons, each of which is formed by the three vertices of the triangle and the three centroids of its neighboring triangles. The CE and SE associated with the centroid mesh point (j, n) of triangle ΔDFB are shown in Fig. 3, in which G, D, F, B, G', D', F', B', G'', D'', F'', and B'' denote mesh points (j,n), (j,n;1), (j,n;2), (j,n;3), ($j,n-1$), ($j,n-1$;1), ($j,n-1$;2), ($j,n-1$;3), ($j,n+1$), ($j,n+1$;1), ($j,n+1$;2), and ($j,n+1$;3), respectively. The conservation element CE(j,n) is a hexagonal cylinder in the E_3-space, while the solution element SE(j, n) is the union of three vertical plane segments, a horizontal plane segment, and their immediate neighborhoods. Note that any domain in the E_3-space can be filled with the CEs defined above if the computational domain is large enough. Since $\overline{FB}$, $\overline{BD}$, and $\overline{DF}$ are opposite to vertices D, F, and B, respectively, whose vertex indices in ΔDFB are $r = 1, 2$, and 3, the cell numbers of the three triangles with

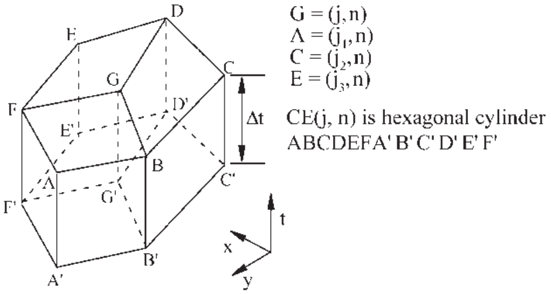

(a) Conservation Element CE(j,n).

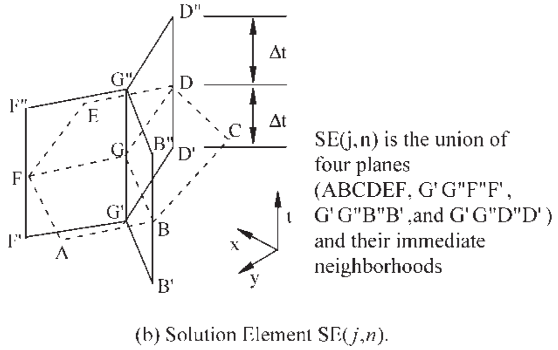

(b) Solution Element SE(j,n).

FIGURE 3 CE and SE associated with centroid mesh point (j, n) of triangle of ΔDFB.

points A, C, and E as their respective centroids are denoted by j_1, j_2, and j_3, respectively. It follows that the mesh indices of points A, C, E, A', C', and E' are (j_1, n), (j_2, n), (j_3, n), $(j_1, n-1)$, $(j_2, n-1)$, and $(j_3, n-1)$, respectively.

Let s_j be the area of hexagon $ABCDEF$ associated with the centroid mesh point j, and $s_j^{(r)}$ $(r = 1, 2, 3)$ the areas of quadrilaterals $GFAB$, $GBCD$, and $GDEF$. Obviously, $s_j = \sum_{r=1}^{3} s_j^{(r)}$. Let $\Delta\vec{s}_j^{(r,i)}$ be the outward surface vector of side face i $(i = 1, 2)$, whose spatial projection is opposite to vertex r of triangle j. Then $\Delta\vec{s}_j^{(1,1)}$ and $\Delta\vec{s}_j^{(1,2)}$ represent the surface vectors of side faces $FF'A'A$ and $AA'B'B$, respectively, while $\Delta\vec{s}_j^{(2,1)}$ and $\Delta\vec{s}_j^{(2,2)}$ are the surface vectors of side faces $BB'C'C$ and $CC'D'D$, respectively. Similarly, $\Delta\vec{s}_j^{(3,1)}$ and $\Delta\vec{s}_j^{(3,2)}$ are the surface vectors of side faces $DD'E'E$ and $EE'F'F$, respectively. Integration of Eq. (17) over $\mathrm{CE}(j, n)$ leads to the following result

$$Q_j^n - \frac{1}{s_j}\int_{\mathrm{CE}(j,n)} H\,\mathrm{d}V = \mathrm{RHS} \tag{18}$$

where

$$\mathrm{RHS} \equiv \frac{1}{s_j}\left[\sum_{r=1}^{3} Q_{j_r}^{n-1} s_j^{(r)} - \sum_{r=1}^{3}\sum_{i=1}^{2}\left[\vec{h}_j^{(r,i)} \cdot \Delta\vec{s}_j^{(r,i)}\right]\right].$$

Here, $\vec{h}_j^{(r,i)} = (E_j^{(r,i)}, F_j^{(r,i)}, Q_j^{(r,i)})$ is the current-density vector $\vec{h}$ defined on the geometrical center of side face i $(i = 1, 2)$, and $\vec{h}_j = (E_j, F_j, Q_j)$ on the solution point of cell j. In the Euclidean space E_3, the temporal component of the surface vector of any side face vanishes, i.e. $\Delta\vec{s}_j^{(r,i)} = ((s_x)_j^{(r,i)}, (s_y)_j^{(r,i)}, 0)$. Therefore,

$$\vec{h}_j^{(r,i)} \cdot \Delta\vec{s}_j^{(r,i)} = (s_x)_j^{(r,i)} E_j^{(r,i)} + (s_y)_j^{(r,i)} F_j^{(r,i)} \tag{19}$$

where $E_j^{(r,i)}$ and $F_j^{(r,i)}$ can be approximated respectively as follows.

$$\begin{aligned} E_j^{(r,i)} = E_{j_r}^{n-1} &+ (E_x)_{j_r}^{n-1}\left(x_j^{(r,i)} - x'_{j_r}\right) \\ &+ (E_y)_{j_r}^{n-1}\left(y_j^{(r,i)} - y'_{j_r}\right) + (E_t)_{j_r}^{n-1} \cdot \Delta t/2, \end{aligned} \tag{20}$$

$$\begin{aligned} F_j^{(r,i)} = F_{j_r}^{n-1} &+ (F_x)_{j_r}^{n-1}\left(x_j^{(r,i)} - x'_{j_r}\right) \\ &+ (F_y)_{j_r}^{n-1}\left(y_j^{(r,i)} - y'_{j_r}\right) + (F_t)_{j_r}^{n-1} \cdot \Delta t/2. \end{aligned} \tag{21}$$

Here, $(x_j^{(r,i)}, y_j^{(r,i)}, (n - 1/2)\Delta t)$ is the coordinate of the geometrical center of side face i whose spatial projection is opposite to vertex r of triangle j, while (x'_{j_r}, y'_{j_r}) is the spatial coordinate of the solution point of cell j_r.

As in the one-dimensional case, Eq. (18) is only a function of Q_j^n and can nominally be solved. After Q_j^n becomes available, $(Q_x)_j^n$ and $(Q_y)_j^n$ can be obtained using the oscillation-suppressing procedure detailed by Wang and Chang (1999).

Treatment of Chemical Source Terms: Subtime-Step Technique

The solution to Eq. (13) for one-dimensional problems or to Eq. (18) for two- dimensional problems requires the integration of chemical source terms over the conservation element $\mathrm{CE}(j,\ n)$. A fully implicit treatment of this integration using an iteration scheme such as the Newton-Raphson method gives rise to numerical difficulties associated with the resultant non-linear equation. This can be attributed to the wide variety of time scales involved. For chemical reaction systems with fast chemistry, such as hydrogen/oxygen mixtures, the characteristic chemical reaction time is smaller than the flow residence time by several orders of magnitude. Thus, these time scales must be carefully treated to ensure the convergence and accuracy of numerical calculations.

To see this clearly, consider a chemically reacting system under a zero-flow condition. Eq. (13) reduces to the following form

$$Y_i^n - \int_{\Delta t} \dot{\omega}_i\,\mathrm{d}t = Y_i^{n-1}. \tag{22}$$

A fully implicit treatment of the source term in Eq. (22) leads to

$$Y_i^n - \Delta t\,\dot{\omega}_i\left(Y_j^n\right) = Y_i^{n-1}. \tag{23}$$

In general, $\dot{\omega}_i$ is a highly non-linear function of Y_j's $(j = 1, \cdots, N_s)$. As a further simplification, consider herein a binary system with a single-step global reaction, i.e., reactant → product. For this particular case $\dot{\omega}_i$ is only a function of the reactant mass fraction. When the time step is small enough (i.e., $\Delta t\dot{\omega}_i$ being relatively smaller than Y_i), the Newton-Raphson iteration formulation for Eq. (23) becomes monotonic with Y_i. This property leads to a successful iteration procedure with a quadratic convergence rate. The monotonicity property vanishes, however, when a large time step is used, due to the presence of local minima and maxima in the course of iteration. The Newton-Raphson scheme consequently may fail, and under-relaxation is required in each iteration loop. It is worth noting that the sign of the source term for a binary system changes synchronously with that of the reactant species concentration. The species concentration remains non-negative in the iteration process and therefore facilitates convergence of the iteration.

Although the Newton-Raphson iteration scheme may function smoothly for a single binary system with small time marching steps, it becomes invalid for multi-component systems with second- or higher-order chemical reactions. The hyperspace formed by the species mass fractions, Y_is, may have many local minimum, maximum, and saddle points when a large time step is employed for temporal integration. Moreover, the self-correction mechanism present in single-step global reactions does not hold for second- or higher-order chemical reactions. The signs of source terms may not follow those of species fractions. Numerical experiments have shown that under-relaxation is not sufficient to correct this ill behavior of the Newton-Raphson iteration caused by the existence of the extreme points in the hyperspace. One way to bypass this difficulty is the use of small numerical time steps comparable to chemical reaction time scales. This approach, however, may render the numerical computation a formidable task for many practical applications. Another compounded disadvantage lies in the high numerical dissipation associated with a small CFL number due to the use of a small time step.

To circumvent these difficulties while retaining the merits of high accuracy and stability of the space–time method, an effective integration scheme based on the subtime-step technique is developed as follows.

$$\int_{\mathrm{CE}(j,n)} H\,\mathrm{d}V \cong s_j \cdot \frac{\Delta t}{N_t}\left(\sum_{n_t=0}^{N_t-1} H_j^{n-n_t}\right) \tag{24}$$

where N_t is the number of sub-time steps within Δt. Equation (24) introduces a new time scale $\Delta t/N_t$ in addition to Δt. The idea underlying Eq. (24) is to use small time steps for chemical reactions, whereas a large CFL number on the order of unity is employed when flow equations are solved. With small time increments within each Δt, the highly non-linear behavior of the chemical source terms can be effectively treated, and the stiff variations of source terms can be properly resolved. Obviously, N_t is dependent on the specific chemical kinetics involved. For flows in which chemical reactions are confined in a small region, N_t may be treated as a spatial function to save computational effort.

Substitution of Eq. (24) into Eq. (18) leads to the following equation

$$Q_j^n = \frac{\Delta t}{N_t}\left(\sum_{n_t=0}^{N_t-1} H_j^{n-n_t}\right) + \mathrm{RHS}. \tag{25}$$

It can be solved using the procedure given below

$$Q_j^0 = \mathrm{RHS}, \tag{25a}$$

$$Q_j^1 = \frac{\Delta t}{N_t} H_j^1 + Q_j^0, \tag{25b}$$

$$\vdots$$

$$Q_j^{N_t} = \frac{\Delta t}{N_t} H_j^{N_t} + Q_j^{N_t-1} \tag{25c}$$

$$Q_j^n = Q_j^{N_t}. \tag{25d}$$

Note that the chemical source terms in Eqs. (25b) and (25c) are treated implicitly, and the Newton-Raphson iteration technique may be employed to solve these subtime steps.

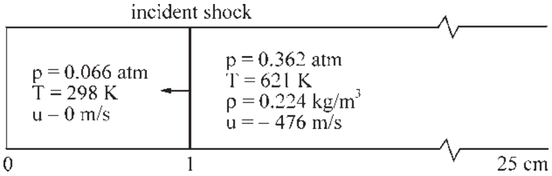

FIGURE 4 Geometry and initial conditions for case of incident shock-induced detonation.

SAMPLE CALCULATIONS

A series of numerical tests has been conducted to validate the accuracy and robustness of the present numerical scheme. The flow fields studied involve strong shock and detonation waves with detailed chemical kinetics. This section presents some representative results, including one-dimensional detonation initiated by shock waves. The ability to treat multi-dimensional detonation problems is also demonstrated.

Incident Shock-Induced Detonation

The first example was taken from the work of Oran *et al.* (1982) on a detonation initiated by an incident shock of a Mach number of 2.165 in a reactive system containing hydrogen/oxygen/argon (molar fraction: 2:1:7) at 0.066 atm and 298 K. Figure 4 shows the geometry and initial conditions used in the simulation. The tube is 25 cm long, and the incident shock is initially located at $x = 1$ cm. The left-end boundary is a reflecting solid wall, and a constant inflow of the fresh reactant mixture moving in at the incident shock velocity is adopted at the right-end boundary. The present case did not consider a full shock-tube problem in order to minimize computational cost. This practice is valid as long as throughout the calculated time span the reflected shock wave remains well separated from the contact discontinuity formed when the diaphragm initially bursts.

Calculations were carried out with a spatially uniform grid of $\Delta x = 0.1$ mm and a CFL number of 0.8. The chemical kinetics model involved nine species (i.e., H_2, O_2, OH, H_2O, H, O, HO_2, H_2O_2, and Ar) and twenty-four elementary reactions (Franklach *et al.*, 1995). Figure 5 shows the time evolution of the maximum pressure in

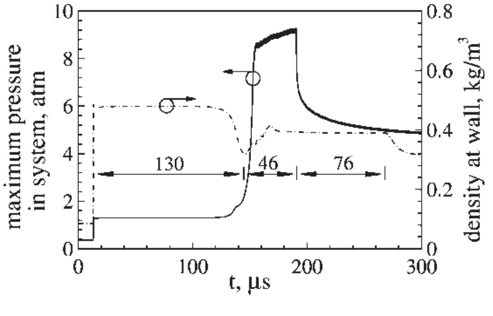

FIGURE 5 Time evolution of maximum pressure in chamber and density at reflecting wall.

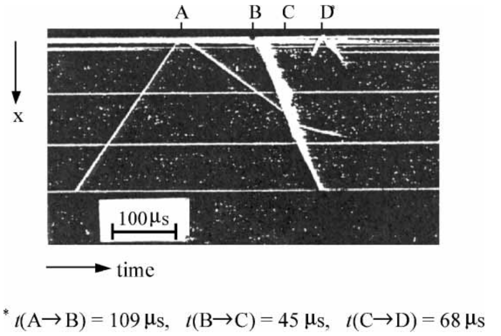

FIGURE 6 Time-resolved Schlieren photograph of shock reflection-reaction wave formation process: A, shock reflection at the wall; B, reaction wave formation at the reflecting wall; C, second emission pulse; D, peak absorption (Oran *et al.*, 1982).

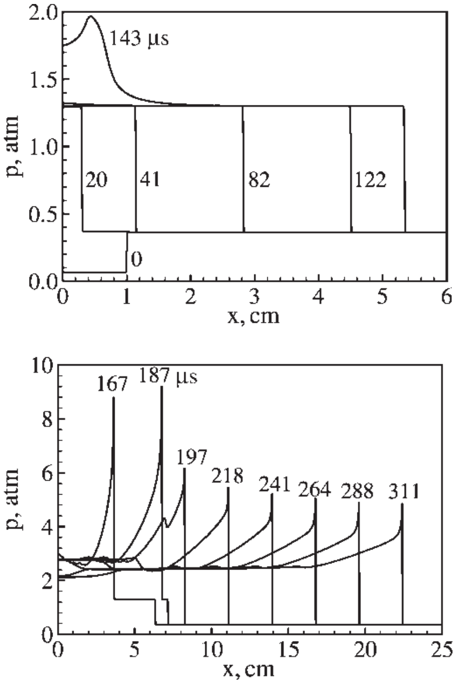

FIGURE 7 Pressure distributions in chamber at various times.

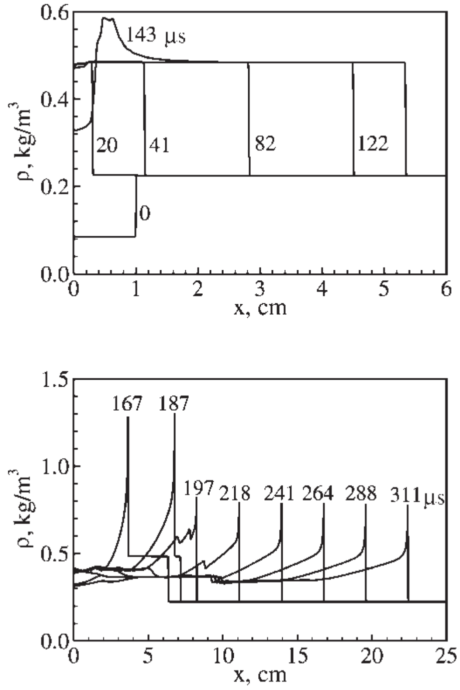

FIGURE 8 Density distribution in chamber at various times.

the chamber and the density at the reflecting wall. For validation, the time-resolved Schlieren photograph taken in the experiment (Oran *et al.*, 1982) is shown in Fig. 6. The maximum pressure remains constant until the incident shock is reflected at 14 μs, which corresponds to moment A in Fig. 6, at which point the pressure jumps to a higher value of 1.3 atm. A reaction wave is then initiated at 144 μs (moment B) after a chemical induction delay of 130 μs. The pressure reaches its maximum at 190 μs (moment C) when the reaction wave and the reflected shock merge. The merged waves result in a rarefaction wave that propagates backward to the wall. At 266 μs (moment D) the rarefaction wave reaches the reflecting wall, leading to a decrease in density at the wall. A comparison of Figs. 5 and 6 shows that the characteristic times obtained from the present numerical study agree closely, if not exactly, with the experimental data. The discrepancies can be attributed to measurement uncertainty. Actually, point A in Fig. 6 is slightly later than the exact moment when the incident shock reaches the wall. Similarly, point D in Fig. 6 is not the exact moment when the peak absorption occurs. The same problem was numerically studied by Oran *et al.* (1982). They adopted a splitting technique with the hydrodynamic part solved with the FCT algorithm. The times they obtained for merging of the shock and reaction waves and the reflection of the reaction wave from the wall differ from experimental results, although the sum of the two times matches the measured value.

More detailed information about the flow evolution can be found in Figs. 7 and 8, which show the spatial distributions of the pressure and density fields at various times, respectively. The different stages of detonation initiation can be clearly identified and examined. The detonation wave velocity derived from the trace of the wave front is $u_D = 1686$ m/s, which is very close to the value of 1621 m/s predicted by a chemical equilibrium analysis using the NASA CEC code (McBride and Gordon, 1996). The pressure and temperature at the Chapman–Jouguet (C–J) point are 2.72 atm and 2974 K, respectively. The relative errors are less than 5%, as compared with the corresponding CEC results of 2.86 atm and 2983 K.

Stationary Shock-Induced Detonation

The second test example treats a stationary shock-induced detonation in a stoichiometric hydrogen/oxygen

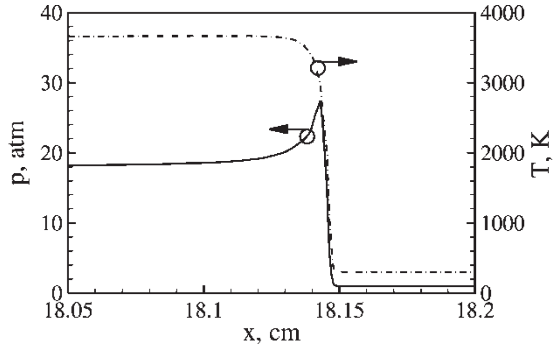

FIGURE 9 Close-up view of pressure and temperature fields near detonation wave front at 64.3 μs.

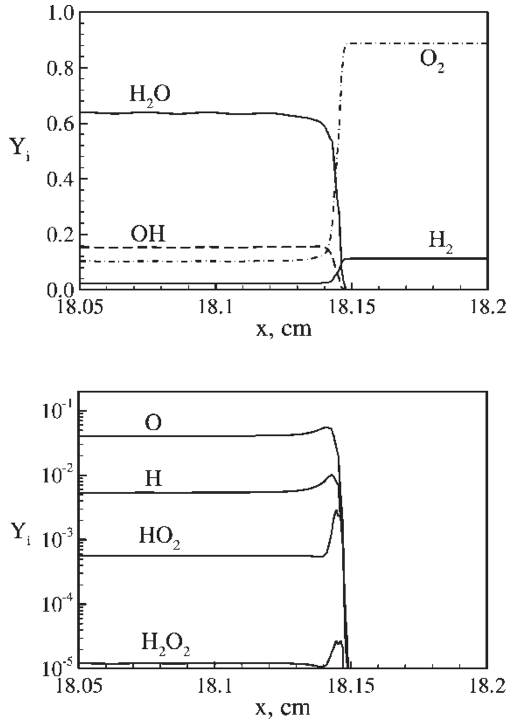

FIGURE 10 Close-up view of species mass fractions near detonation wave front at 64.3 μs.

mixture. The chemical kinetics scheme is basically identical to that in the previous example, except that no inert gas is involved. Detonation in this reactive system is much stronger than that in the first example and therefore poses more severe challenges to numerical schemes in terms of robustness, accuracy, and efficiency.

The physical model under consideration includes a one-dimensional tube measuring 20 cm in length, with the head end closed and downstream end open. The tube is initially filled with a stationary stoichiometric H_2/O_2 mixture at 1 atm and 300 K. A driver section covering a length of 0.2 cm with $p_{\text{driver}} = 30$ atm and $T_{\text{driver}} = 3000$ K is introduced at the head end to initiate detonation. The species concentrations of the driver gas are determined from the chemical equilibrium calculation (McBride and Gordon, 1996) for the reactant mixture at p_{driver} and T_{driver}. Two different mesh systems are employed in the numerical simulation. The baseline grid has a size of $\Delta x = 0.01$ cm uniformly distributed throughout the entire computational domain. A refined grid with a size of $\Delta x/12$ is used to cover a small region around the detonation wave front to enhance the local resolution. The flow conservation across the grid interfaces is ensured using a technique recently developed within the framework of the space–time method (Chang *et al.*, 2001). Calculations were conducted with a CFL number of 0.5 based on the coarse grid. Figures 9 and 10 show the close-up views of the pressure, temperature, and species mass-fraction fields near the detonation wave front at 64.3 μs. Excellent resolution is achieved, demonstrating the effectiveness of the present scheme and the local mesh refinement technique. The calculated detonation wave velocity obtained by tracing the wave front is 2801 m/s, compared to 2837 m/s as predicted by the chemical equilibrium calculation. The C–J properties are derived from the numerical results based on the requirement that the local Mach number be unity at the C–J point. The discrepancy between the results of the present analysis and the chemical equilibrium calculation is less than 5%, as shown in Table I.

Detonation in Two-dimensional Configuration

A two-dimensional flow involving detonation initiation and propagation was simulated as the third example problem. The detonation tube adopted in the calculation has a length of 60 cm. The head end is closed, and a convergent-divergent nozzle of a length of 20 cm is attached to the tube exit. The slopes of the convergent and divergent parts of the nozzle are 45 and 15 degrees, respectively, and the diameters of the nozzle inlet, throat, and exit are 16, 12, and 20 cm, respectively.

The computational domain included the tube, nozzle, and external region and was discretized using an unstructured grid (Wang and Chang, 1999). The reactive system of concern was a stoichiometric H_2/air mixture. The ZND model was adopted in the current case, i.e.,

TABLE I Detonation properties for stoichiometric H_2/O_2 system at 1 atm and 300 K

	u_D, m/s	p_{CJ}, atm	T_{CJ}, K	$Y(H_2)$	$Y(O_2)$	$Y(H_2O)$
Chemical equivalence	2837	18.7	3681	0.0226	0.1066	0.6644
Present	2801	17.5	3650	0.0217	0.1025	0.6394
Relative error	1.3%	4.8%	0.8%	4.0%	3.8%	3.7%

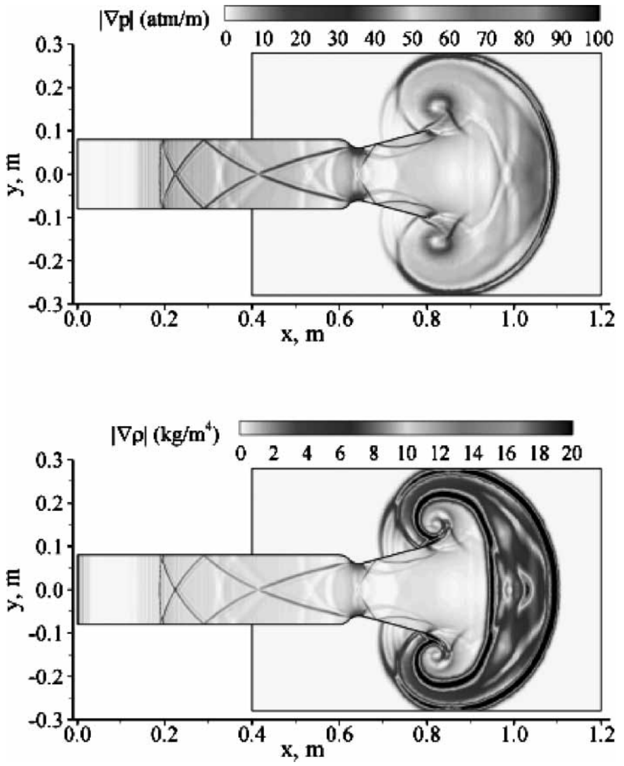

FIGURE 11 Snapshots of pressure and density gradient fields at 0.80 ms.

reactants and products were, respectively, lumped into two distinct species with similar molecular weights ($\mathrm{MW} = 22.54\,\mathrm{g/mol}$) and thermodynamic properties (specific heat ratio $\gamma = 1.29$). The mass production rate of the reactant was

$$\dot{\omega} = -K\rho Z \exp(-E_\mathrm{a}/T) \tag{26}$$

where Z, $E_\mathrm{a} = 4.794 \times 10^6\,\mathrm{J/kg}$, and $K = 7.5 \times 10^9\,\mathrm{s}^{-1}$ are the reactant mass fraction, activation energy, and pre-exponential reaction rate factor, respectively. The heat release per unit mass of reactant for the current system was $q = 2.720 \times 10^6\,\mathrm{J/kg}$. The tube was initially filled with the reactant, with the nozzle section and external field containing air. A stationary shock with a length of 0.2 mm and $p_\mathrm{driver} = 30$ atm and $T_\mathrm{driver} = 2500$ K was employed to initiate detonation. Figure 11 shows snapshots of the pressure and density gradient fields at 0.80 ms. Two bow shocks were generated in the tube when the detonation reached the nozzle entrance. They moved backward and interacted with each other, leading to a normal shock wave propagating upstream. In the external field, the strength of the primary shock decreased very quickly due to the rapid flow expansion. Two vortices were developed as the shock deflected over the edge of the nozzle exit. The well-resolved flow structures clearly demonstrate the capability of the present scheme in solving multi-dimensional flows with discontinuities and strong source terms. A more detailed discussion of this subject is given by Wu *et al.* (2003).

CONCLUSIONS

A new scheme based on the space–time CE/SE method has been developed for treating multi-component chemically reacting flows with detailed chemical kinetics. The conservation equations of mass, momentum, energy, and species concentration are discretized using the space–time method, and the time evolution of chemical source terms is integrated using a subtime-step technique. The scheme is capable of solving flows with intensive chemical reactions and strong gradients, as demonstrated by numerical experiments on several detonation problems. The local mesh refinement algorithm is also shown to perform effectively in terms of numerical efficiency and accuracy.

Acknowledgements

The authors are deeply indebted to Dr S.C. Chang and Dr K.C. Hsieh for their technical advice and support during the course of this research. This work was supported partly by the Pennsylvania State University and partly by the DoD Multidisciplinary University Research Initiative under ONR Grant No. N00014-99-1-0744, with Dr Gabriel Roy serving as the program manager.

References

Boris, J.P. and Book, D.L. (1973) "Flux-corrected transport I: SHASTA, a fluid transport algorithm that works", *Journal of Computational Physics* **11**, 38–69.

Boris, J.P. and Oran, E.S. (2001) Numerical Simulation of Reactive Flow (Cambridge University Press, New York/Cambridge).

Chang, S.C. (1995) "The method of space–time conservation element and solution element—a new approach for solving the Navier–Stokes and Euler equations", *Journal of Computational Physics* **119**, 295–324.

Chang, S.C., Loh, C.Y., Yu, S.T., Himansu, A., Wang, X.Y. and Jorgenson, P.C.E. (1997) "Robust and simple non-reflecting boundary conditions for the space–time conservation element and solution element method", *AIAA Paper 1997–2077, AIAA Computational Fluid Dynamics Conference, Snowmass Village, Colorado*.

Chang, S.C., Yu, S.T., Himansu, A., Wang, X.Y., Chow, C.Y. and Loh, C.Y. (1998) "The method of space–time conservation element and solution element—a new paradigm for numerical solution of conservation laws", Computational Fluid Dynamics Review 1998 (World Scientific, Singapore) Vol. **1**.

Chang, S.C., Wang, X.Y. and Chow, C.Y. (1999) "The space–time conservation element and solution element: a new high resolution and genuinely multidimensional paradigm for solving conservation laws", *Journal of Computational Physics* **156**, 89–136.

Chang, S.C., Wu, Y., Wang, X.Y. and Yang, V. (2001) "Local mesh refinement in the space–time CE/SE method", Computational Fluid Dynamics 2000, Proceedings of the First International Conference on Computational Fluid Dynamics (ICCFD) (Springer-Verlag, New York), pp 61–66.

Franklach, M., Wang, H., Goldenburg, M., Smith, G.P., Golden, D.M., Bowman, C.T., Hanson, R.K., Gardiner, W.C. and Lissianski, V. (1995) GRI-Mech–An Optimized Detailed Chemical Reaction Mechanism for Methane Combustion (Gas Research Institute), Technical Report GRI-95/0058.

Guo, Y., Hsu, A.T., Yang, Z. and Oyediran, A. (2000) "Numerical Simulation of 2D Combustion Flows with the CE/SE Method", *AIAA Paper 2000-0865, AIAA, 38th Aerospace Sciences Meeting and Exhibit, Reno, Nevada.*

Harten, A. (1984) "On a class of high resolution total-variation-stable finite-difference schemes", *SIAM Journal on Numerical Analysis* **21**(1), 1–23.

Hsieh, S.Y. and Yang, V. (1997) "A preconditioned flux-differencing scheme for chemically reacting flows at all mach numbers", *International Journal of Computational Fluid Dynamics* **8**, 31–49.

LeVeque, R.J. and Yee, H.C. (1990) "A study of numerical methods for hyperbolic conservation laws with stiff source terms", *Journal of Computational Physics* **86**, 187–210.

Li, C., Kailasanath, K. and Patnaik, G. (2000) "A numerical study of flow field evolution in a pulsed detonation engine", *AIAA Paper 2000-0314, AIAA, 38th Aerospace Sciences Meeting and Exhibit, Reno, Nevada*.

Loh, C.Y., Chang, S.C. and Scott, J.R. (1996) "Computational Aeroacoustics via the Space–time Conservation Element/Solution Element Method", *AIAA Paper 1996-1687, 2nd AIAA/CEAS Aeroacoustics Conference, State College, Pennsylvania*.

McBride, B.J. and Gordon, S. (1996) "Computer program for calculation of complex chemical equilibrium compositions and applications", *NASA Reference Publication*, 1311.

Oran, E.S., Young, T.R., Boris, J.P. and Cohen, A. (1982) "Weak and strong ignition. I. Numerical simulations of shock tube experiments", *Combustion and Flame* **48**, 135–148.

Shuen, J.S. (1992) "Upwind differencing and LU factorization for chemical non-equilibrium Navier–Stokes equations", *Journal of Computational Physics* **99**, 233–250.

Shuen, J.S., Liou, M.S. and Leer, B.V. (1990) "Inviscid flux-splitting algorithms for real gases with non-equilibrium chemistry", *Journal of Computational Physics* **90**, 371–395.

Shuen, J.S., Chen, K.H. and Choi, Y. (1993) "A coupled implicit method for chemical non-equilibrium flows at all speeds", *Journal of Computational Physics* **106**, 306–318.

Wang, X.Y. and Chang, S.C. (1999) "A 2-D non-splitting unstructured triangular mesh Euler solver based on the space–time conservation element and solution element", *Journal of Computational Fluid Dynamics* **8**, 309–325.

Wu, Y., Yang, V. and Hsieh, K.C. (1999) "Simulation of unsteady premixed flames with detailed chemical kinetics using the space–time method", *AIAA Paper 1999-1010, AIAA, 37th Aerospace Sciences Meeting and Exhibit, Reno, Nevada*.

Wu, Y.H., Ma, F.H. and Yang, V. (2003) "System performance and thermodynamic cycle analysis of supersonic air-breathing pulse detonation engines", *Journal of Propulsion and Power* **19**(4).

Yu, S.T. and Chang, S.C. (1997) "Treatment of stiff source terms in conservation laws by the method of space–time conservation element and solution element", *AIAA Paper 1997-0435, AIAA, 35th Aerospace Sciences Meeting and Exhibit, Reno, Nevada*.

Yu, S.T., Chang, S.C. and Jorgenson, P.C.E. (1999) "Direct calculation of detonation with multi-step finite-rate chemistry by the space–time conservation element and solution element method", *AIAA Paper 1999-3772, AIAA, 30th Fluid Dynamics Conference and Exhibit, Norfolk, Virginia*.